

SHAKEDOWN AND DYNAMIC BEHAVIOUR OF MASONRY ARCH RAILWAY BRIDGES

Tamás Forgács¹, Vasilis Sarhosis², Sándor Ádány¹

¹*School of Civil Engineering, University of Leeds, Leeds, LS2 9JT, UK*

²*University of Technology and Economics, H-1111 Budapest, Műegyetem rkp. 3, Hungary*

Abstract

Masonry arch bridges form an integral part of our rail infrastructure network and their safety is important for the functioning of our society. Although, there have been several studies to understand the in-service condition of masonry arch bridges, these are mainly focusing on static analyses. However, it is well known that moving vehicles exert a dynamic force on bridges as they cross them. This paper investigates the shakedown and dynamic behaviour of railway masonry arch bridges under traffic load conditions. A nonlinear, mixed discrete-finite element numerical model was developed to investigate static and dynamic response on a masonry arch bridge. Each voussoir of the masonry arch was represented by a distinct block, while the mortar joints were modelled as zero thickness interfaces which can open and close depending on the magnitude and direction of the stresses applied to them. Both static and real dynamic analyses were carried out investigate the effects of moving traffic loads. In addition, investigations into the train to bridge interaction were undertaken and the dynamic amplification factors (DAFs) were estimated. From the evaluation of the results, it was shown that as the external load passes through the bridge, plastic deformations and residual stresses exist in the arch barrel. Also, the dynamic amplification depends on the magnitude of the external load. As the load increases, non-linearity in the structure is evident, which decreases the natural frequency of the bridge. Hence the critical speed is decreasing. Observations provided here reveal new insight into the residual and load carrying capacity of masonry arch bridges.

Keywords: Masonry arch bridge, dynamic analysis, plastic shakedown, moving load, discrete element method, railway bridges

40 1. Introduction

41 Europe is sustained by a highly complex and interconnected network of transport infrastructure.
42 Masonry arch bridges forms the backbone of European transport infrastructure network (e.g. there are
43 approximately 200,000 masonry arch bridges still in use on the European railway network [1]) and their
44 reliability and integrity is vital for ensuring economic activity and prosperity. The majority of masonry
45 arch bridges were built in the 19th century, in parallel with the industrial revolution [2]. Today, these are
46 still in-service but showing significant signs of distress. Weathering, demands of increasing axle loads
47 and train velocities [3], plus factors such as increased frequency of flood events due to climate change
48 have introduced extreme uncertainty in the long-term performance of such infrastructure assets. Also,
49 much of our masonry infrastructure has significant heritage and cultural value and in many countries
50 have a policy to “retain and repair”, rather than “demolish and replace” them [4]. Failure of such
51 infrastructure could lead to direct and indirect costs to the economy and society and hamper rescue and
52 recovery efforts. From the above, there is an imperative need to better understand the mechanical
53 behaviour of masonry arch bridges and provide detailed and accurate data that will better inform
54 maintenance programmes and asset management decisions. Without a strategic approach to caring for
55 our ageing masonry infrastructure, we run the risk of over-investing in some areas while neglecting
56 others that are in need of our attention.

57 However, assessing the structural performance of ageing masonry infrastructure is a complex task.
58 Previous research has clearly demonstrated that the assessment methods currently used by the industry
59 are antiquated and/or over-simplistic. For example, for the assessment of masonry arch bridges, the
60 Military Engineering Experimental Establishment (MEXE) method of assessment is still in use
61 especially in UK. This is a semi-empirical approach based on an elastic analysis by Pippard et al. [5]
62 who modelled the arch barrel as linear elastic, segmental in shape, pinned at its support and carrying a
63 central point load. The method dates back to the 1940s, has very limited predictive capability, and offers
64 little scope for future enhancement [6]. Other assessment approaches used by the industry (particularly
65 in the UK) are: a) the static theorem of plastic limit analysis (developed into the Archie-M software)
66 which uses simple equilibrium calculations (the self-weight of the arch barrel and live loads are balanced
67 by forces between the blocks); and b) the RING software which is based on the rigid block theory and
68 uses the kinematic theorem of limit analysis to identify the collapse state with the smallest external
69 loading and hence predict the ultimate load [7]. Although the primary focus of these methods has been
70 on the prediction of structural failure of ageing masonry infrastructure, prediction of the service load
71 above which incremental damage occurs is now a key priority for infrastructure owners, who are under
72 increasing pressure to provide transport networks which are secure and resilient [8].

73 Over the last three decades, significant efforts have been devoted to the development of numerical
74 models to represent the complex and non-linear in-service behaviour and limit state capacity of masonry
75 structures subjected to external loads. Such models range from considering masonry as a continuum
76 (macro-models) to the more detailed ones that consider masonry as an assemblage of units and mortar
77 joints (micro-models/meso-scale models); see Boothby [9] and Sarhosis et al. [10]. In particular, Choo
78 and Gong [11] have successfully used the Finite Element Method (FEM) to developed models of
79 masonry arch bridges to predict their ultimate load carrying capacity. However, in macro-models based
80 on the FEM, the description of the discontinuity is limited since they consider the arch as a continuum
81 element [10, 12]. An overview of such models can be found in Boothby [13] and Sarhosis et al. [10].
82 Given the importance of the masonry unit-to-mortar interface [14, 15] on the structural behaviour of
83 aged masonry arch bridges, micro-modelling approaches (i.e. those based on Discrete-Finite Element
84 Method) are better suited to simulating their serviceability and load carrying capacity [16-18].
85 Sophisticated FEM approaches (e.g. those based on the contact element techniques) were able to reflect
86 the discrete nature of masonry e.g. those presented by Fanning and Boothby [9], Gago et al. [19], Ford
87 et al. [20] and Drosopoulos et al. [21]. However, such methods require high computational cost, are
88 unable to realistically predict the crack development at serviceability limit state and have convergence
89 difficulties when blocks fall or slide excessively. Another modelling approach is the one described by

90 the fibre-beam approach which can predict the collapse mechanism of masonry and to account for the
91 effective material behaviour with acceptable computational effort. According to the method, the
92 masonry arch can be modelled as a segmental fibre-beam [22]. The approach has been successfully used
93 to study the behaviour of masonry arches and arch bridges under static and dynamic conditions [23].
94 Despite the simplifications in the representation of structural geometry, it was found a promising
95 approach for preliminary assessment of the seismic capacity of masonry arch bridges.

96 An alternative and attractive method in which the discrete nature of the masonry can be more realistically
97 represented is the Discrete Element Method (DEM). The advantage of the DEM is that it considers the
98 arch as a collection of separate voussoirs able to slide and rotate relative to each other. The DEM was
99 developed by Cundall [24] to model blocky-rock systems and sliding along rock mass. The approach
100 was recently implemented to simulate the mechanical response of masonry structures including arches
101 [14, 16, 25-27] in which failure occurs along mortar joints. From past studies carried out using DEM to
102 simulate the mechanical response of masonry arch bridges, it was found that the method is suitable and
103 reliable especially in the case in which failure is dominated at masonry unit-to-mortar interface [12].
104 Also, an important finding from past literature review studies presented by Sarhosis et al. [10] is that the
105 majority, if not all, of the past research is focusing on the behaviour of masonry arch bridges subjected
106 to static loads. In such studies, to reach conclusions related to the load carrying capacity of masonry
107 arch bridges, an increasing in magnitude point load is applied at the quarter and/or at mid-span of the
108 masonry arch bridge.

109 However, vehicles crossing masonry arch bridges are exerting dynamic loads on them. Most of the
110 standards and industry guidelines [1, 3, 28, 29] suggest the use of dynamic amplification factors to take
111 into account such effects. In this case, static analysis can be carried out, while the static response of the
112 structure (e.g. displacements, internal forces, stresses) should be multiplied by the dynamic
113 amplification factor. In this way, real dynamic analysis can be avoided. Also, there are several analytical
114 [30], numerical [31-34] and experimental [35] studies investigating the dynamic response of masonry
115 arch bridges. Smith and Acikgoz [30] investigated the dynamic behaviour of linear elastic curved beams.
116 Partial differential equations of the vibration were derived and solved numerically. Dynamic
117 amplification factors were determined. According to the authors, codified procedures can significantly
118 underestimate the dynamic amplification. In addition, Ataei et al. [35] estimated the dynamic
119 amplification factors of eleven multi-span masonry arch bridges. Vertical deflection of the crown was
120 measured when different in speed and weight train crossed the bridge. Moreover, due to the importance
121 of this subject, many guidelines are provided by various codes and design standards (e.g. ERRI-D214
122 [36]) for designing and performance assessment on the dynamic characteristics of bridges. However,
123 from the above studies it is evident that assessing the in-service condition of masonry arch bridges is a
124 rather difficult task. This is mainly due to the complexity of the problem and that recent studies have
125 reported contradictory results.

126 This paper aims to study the dynamic phenomena on masonry arch bridges due to vehicle load. A
127 numerical model has been developed to analyse both static and dynamic response of masonry arch
128 bridges with the purpose of estimating the traffic effects by means of moving loads. As a case study, the
129 geometrical characteristics of the Prestwood bridge have been adopted in the investigations. The
130 structural assessment and numerical analyses of the bridge were performed based on a detailed finite-
131 discrete element code. Suitable constitutive laws were considered for the mortar joints and for the
132 backfill. The numerical results were compared against field test results. The interaction between the
133 train and the track is considered through a simplified methodology. Two different types of static analyses
134 (incrementally increased load at fixed points and quasi-static moving load) and real dynamic analysis
135 were carried out. In addition, dynamic amplification factors (DAFs) were estimated. Results of this study
136 were used to assess how train load and train speed affect the DAF on a masonry arch bridge.

137 **2. Current dynamic amplification factors for railway bridges**

138 The passage of trains on bridges exerts dynamic effects on them. Dynamic effects are able to change the
 139 structural response (e.g. the displacements, internal forces etc.) of a bridge. According to Eurocode [28],
 140 the extent of the dynamic effects on bridges depends mainly on: a) the velocity of the train; b) the number
 141 and weights of the axles; c) the span of the bridge; and d) the natural frequency (mass and stiffness) of
 142 the bridge. Other factors which may influence the dynamic effect in bridges are the railway track to train
 143 interaction and the dynamic characteristics of the ballast; but these effects are out of scope of this work.
 144 The simplified method of Eurocode (EN 1991-2:2003) for railway bridges enables the engineer to carry
 145 out static analysis with LM71 vertical load model and multiply the structural response with the dynamic
 146 amplification factors calculated as:

$$\Phi_2 = \frac{1.44}{\sqrt{L_\phi - 0.2}} + 0.82 \quad 1.00 \leq \Phi_2 \leq 1.67, \quad (1)$$

$$\Phi_3 = \frac{2.16}{\sqrt{L_\phi - 0.2}} + 0.73 \quad 1.00 \leq \Phi_3 \leq 2.00, \quad (2)$$

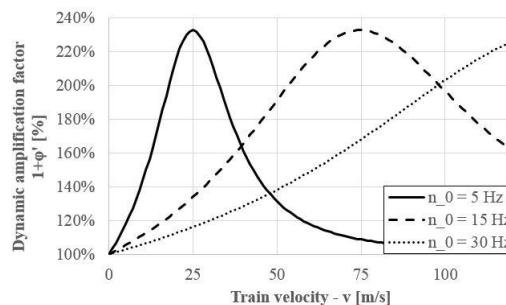
147 where L_ϕ is the determinant length in meters (see EN 1991-2: Traffic load on structures), while Φ_2
 148 and Φ_3 are the dynamic factors for carefully maintained tracks and tracks with standard maintenance,
 149 respectively. These formulas can only be used if: a) the first natural frequency of the structure does not
 150 exceeds the lower and upper-limit for natural frequency defined in the standard; and b) the train velocity
 151 does not exceed 200 km/h (56 m/s). It should be noted that the dynamic amplification of EN 1991-2
 152 simplified method does not depend on the velocity of the train.

153 EN 1991-2 Annex C [28], Network Rail [29] and UIC suggest another method to calculate the dynamic
 154 amplification factor (Eq. (3) and (4)). This method takes into account not just the span and the first
 155 natural frequency of the structure, but the velocity of the train as well. The dynamic enhancement can
 156 be calculated as:

$$\varphi' = \frac{K}{1 - K + K^4} \quad (3)$$

$$K = \frac{v_x}{2n_0 L_\phi} \quad (4)$$

157 where v_x is the velocity of the train in meters per second, L_ϕ is the determinant length in meters and
 158 n_0 the first natural frequency of the bridge in Hz. Equations (3) and (4) were determined in the 60's to
 159 conservatively characterize the dynamic response of simple supported concrete and steel bridges [37].
 160 To handle the different mode shapes of the different structural systems, determinant length (L_ϕ) was
 161 introduced. In the case of single span arch bridges, the determinant length should be the half of the span.
 162 In Figure 1, the DAF were calculated for a 6.55 m single span arch bridge with various natural
 163 frequencies according to Eqs (3) and (4).



164 Figure 1 – Dynamic Amplification Factor according to Network Rail [29]
 165

166 **3. The proposed mixed discrete-continuum approach to evaluate the dynamic response of**
167 **masonry arch bridges**

168 Understanding the mechanical behaviour of masonry arch bridges is a challenging task for an engineer.
169 Even under static conditions, the mechanical behaviour of masonry arch bridges is complex and the
170 analytical tools available by engineers to assess the life expectancy of such bridges needs refinement.
171 The selection of the most appropriate computational method to use for the analysis of masonry
172 structures, among other factors, should include representation of joint opening between voussoirs in the
173 arch; sliding between the arch barrel and the soil, plastic response in the backfill above the arch etc. In
174 case of dynamic analysis, in addition to the aforementioned factors, the computational model should
175 include inertial and vehicle-structure interaction effects.

176 To computationally evaluate the dynamic response of masonry arch bridges, the mixed discrete-
177 continuum element code UDEC, developed by ITASCA has been used in this study. Within UDEC,
178 voussoirs in the barrel vault were represented by distinct linear-elastic deformable blocks separated by
179 zero thickness interfaces at each mortar joint. The voussoirs were subdivided into finite elements so that
180 stresses can be calculated. Backfill was represented as a linear elastic-perfectly plastic material.
181 Deformability and non-linear behaviour of backfill was approximated with finite element discretization.
182 The model makes use of an explicit dynamic solution scheme, which makes it able to carry out real
183 dynamic analysis.

184 **3.1. Contact formulation and solution procedure**

185 The discrete elements can interact with each other through zero-thickness interface elements. At the
186 interfaces, blocks are connected kinematically to each other by sets of point contacts [38, 39], along the
187 outside perimeter of the blocks, at locations where corners or edges meet [16]. In the model, large block
188 movements are allowed, including cases of complete detachment and re-closure when external forces
189 are applied to them, with no attempt to obtain a continuous stress distribution through the contact
190 surface.

191 At each contact point, there are two spring connections. These can transfer either a normal force or a
192 shear force from one block to the other. In the normal direction, the mechanical behaviour of the joints
193 (i.e. the zero-thickness contact interface) is governed by the following equation (Figure 2a):

$$\Delta\sigma_n = k_n \Delta u_n, \quad (5)$$

194 where k_n is the normal stiffness of the contact and Δu_n is the increment in normal contact displacement,
195 i.e., the relative displacement between the blocks at the contact point. Similarly, in the shear direction,
196 the mechanical behaviour is controlled by the constant shear stiffness k_s using the following expression
197 (Figure 2b):

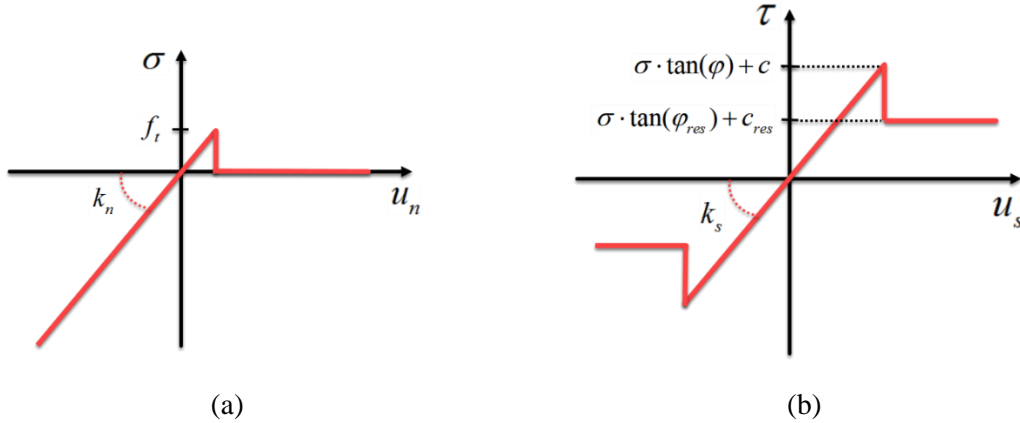
$$\Delta\tau_s = k_s \Delta u_s, \quad (6)$$

198 where $\Delta\tau_s$ is the change in shear stress, and Δu_s is the increment in shear displacement.

199 In the present research work, the contacts are assumed to follow the Mohr-Coulomb failure criterion,
200 commonly used to represent shear failure in soils and rocks. The criterion has a limiting tensile strength,
201 f_t . If the contact normal stress exceeds the tensile strength, then the normal stress is set to zero and the
202 interface opens. Alternatively, at those contacts undergoing compression, a small overlap will occur
203 between block edges (Figure 2a). The amount of overlap is controlled by the normal stiffness. Similarly,
204 in shear, in the elastic range, the response is controlled by contact shear stiffness (Figure 2b). In addition,
205 in the shear direction, slippage between blocks occurs when the tangential or shear stress at a contact
206 exceeds a critical value τ_{\max} defined by:

$$|\tau_s| \leq c + \sigma_n \tan(\varphi) = \tau_{\max}, \quad (7)$$

207 where $\mu = \tan(\varphi)$ is the friction coefficient and φ the angle of friction and c the cohesive strength.
 208 After slip takes place, the shear stress is reduced according to the Mohr-Coulomb criterion, but using
 209 residual values for cohesion (c_{res}) and friction (φ_{res}), as shown in Figure 2b. Non-associative flow rule
 210 is applied therefore the dilation angle (ψ) is set to zero. After a contact breaks or slips, forces are
 211 redistributed, and it might cause adjacent contacts to break.



212
 213
 214 Figure 2 –Mechanical behaviour of contacts in (a) normal and in (b) shear direction

215 In the presented model, the Newtonian equations of motion are solved directly by the UDEC with an
 216 explicit time stepping algorithm. The explicit scheme applies the central difference method. As a result,
 217 velocity of each node can be calculated. With the help of nodal velocities, displacements and location
 218 of the nodes can be updated. After the new position of the elements is known, contact locations and
 219 orientation can be calculated. Contact forces are updated by invoking the contact constitutive law, as
 220 described in the previous section. For the internal finite elements, nodal displacements lead to new
 221 strains, from which zone stresses ensue by applying the assumed material constitutive model. In this
 222 way, nodal forces can be assembled for the next calculation step.

223 The central difference method is only conditionally stable. To avoid numerical instabilities arising from
 224 calculation of block deformation, a limiting timestep is evaluated for each node. This limiting timestep
 225 is depend on the mass associated with block node; the elastic properties of the block material and the
 226 size of the finite element. Moreover, another limiting timestep for the inter-block relative displacement
 227 should be calculated and it depends on the mass of the smallest block and the maximum contact stiffness
 228 in the system. The geometry of the finite elements can change during the mechanical process, hence the
 229 controlling timestep for the analysis needs to be recalculated in every calculation step.

230 In the case of static analysis, artificial damping is applied to reach equilibrium as fast as possible. Here
 231 the role of the damping is a numerical servo-mechanism to absorb the unwanted elastic oscillations of
 232 the system. While in the case of dynamic simulation, the role of the damping is to model the energy loss
 233 of materials. Energy absorption can develop in plastic material behaviour and with frictional sliding as
 234 well. During dynamic simulations, additional Rayleigh damping was not applied.

235 3.2. Vehicle-structure interaction

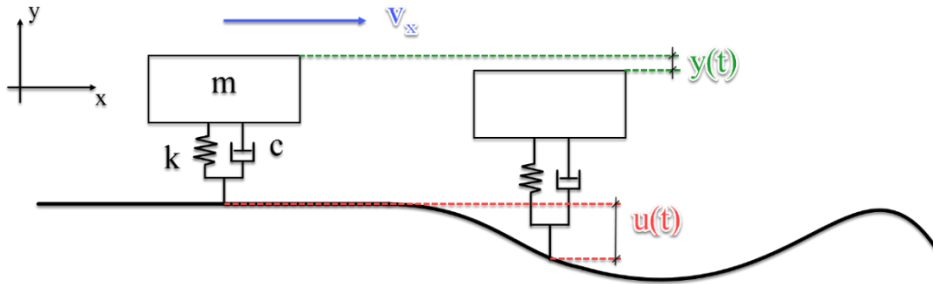
236 Vehicle-structure interaction was implemented into UDEC via FISH programming (embedded
 237 programme language of Itasca software) as a single degree of freedom system (see Figure 3). The
 238 differential equation of the vehicle's motion can be written as:

$$m\ddot{y}(t) + \alpha(t) \left[c (\dot{y}(t) - \dot{u}(t)) + k (y(t) - u(t)) \right] = mg, \quad (8)$$

239 where m is the mass of the vehicle. Spring stiffness and damping coefficient was obtained from [31]:
 240 $k = 159500$ N/m and $c = 0.2 \times 2\sqrt{k \times m}$, respectively. $y(t)$, $\dot{y}(t)$, $\ddot{y}(t)$ are the vertical displacement,
 241 velocity and the acceleration of the vehicle, while $u(t)$, $\dot{u}(t)$ are the vertical displacement, and velocity
 242 of the track. $\alpha(t)$ is intended to represent the possibility of detachment between the vehicle and the
 243 track as follows:

$$\alpha(t) = \begin{cases} 0 & \text{if } k(y(t) - u(t)) + c(\dot{y}(t) - \dot{u}(t)) \geq 0 \\ 1 & \text{if } k(y(t) - u(t)) + c(\dot{y}(t) - \dot{u}(t)) < 0 \end{cases} \quad (9)$$

244 From Equation (9), if the force between the vehicle and the track is in tension, then the differential
 245 equation is reduced to the differential equation of free fall, while the contact force is set to zero.



246
 247 Figure 3 – Single degree of freedom mass-spring-damper model for vehicle-structure interaction

248 The ordinary differential equation described in Equation (8) is solved numerically with the forward
 249 Euler method. The initial conditions are:

$$\begin{aligned} y(0) &= \frac{-mg}{k} & u(0) &= 0 \\ \dot{y}(0) &= 0 & \dot{u}(0) &= 0 \end{aligned} \quad (10)$$

250 The timestep used during solution is equal to the critical timestep determined by UDEC for solution.
 251 The vertical displacement and the velocity of the vehicle are calculated with Equation (11) and (12),
 252 respectively. This calculation process was done simultaneously with the built-in UDEC solution
 253 algorithm applying the same timestep.

$$y(t) = y(t - \Delta t) + \dot{y}(t - \Delta t)\Delta t \quad , \quad (11)$$

$$\dot{y}(t) = \dot{y}(t - \Delta t) + \alpha(t - \Delta t) \left(\frac{mg - c(\dot{y}(t - \Delta t) - \dot{u}(t - \Delta t)) - k(y(t - \Delta t) - u(t - \Delta t))}{m} \right) \Delta t \quad . \quad (12)$$

254

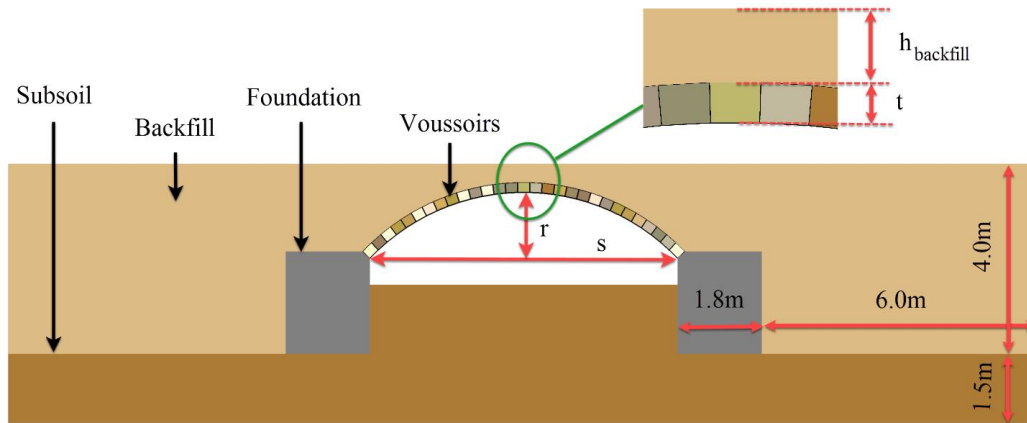
255

256 **4. Development of the numerical model**

257 Although several research, including the one from the authors of this manuscript [40, 41], have been
 258 done in the past to computationally model and understand the three dimensional mechanical behaviour
 259 of masonry arch bridges, the work presented herein uses a 2D mixed discrete-finite element approach.
 260 The reason for adopting a 2D model in this study was to understand better the basic nature of the
 261 investigated phenomena, while the released computational needs enables the authors to use more
 262 accurate (more dense) finite element mesh, and more parametric studies to be carry out in a
 263 computationally efficient manner. By using a 2D model, the possibility to analyse transverse behaviour
 264 (e.g. effect of spandrel walls, transverse load distribution) is dismissed. Moreover, other elements of a
 265 railway bridge like ballast, sleepers and rail were neglected in the model.

266 **4.1. Geometry and materials used for the development of the numerical model**

267 The geometry and material properties of the investigated structure was taken to represent the Prestwood
 268 Bridge, UK. There was no intention to model the foundations and the subsoils in detail. Page [42] carried
 269 out full scale experimental tests on Prestwood Bridge to determine the load bearing capacity of the
 270 structure. The validation of the adopted model against the field scale results is presented in [39]. Details
 271 of the geometry of the model are shown in Figure 4 and in Table 1.



272 Figure 4 – Geometrical characteristic of the numerical model

273 Table 1 – Geometrical characteristic of the bridge

274

Span	Rise	Barrel thickness	Height of the backfill
6.550 m	1.428 m	0.220 m	0.400 m

275 The foundation of the bridge and the voussoirs of the arch ring were assumed to behave in a linear elastic
 276 manner. The backfill of the arch bridge was simulated as linear elastic-perfectly plastic material,
 277 according to Mohr-Coulomb failure criterion. Material properties of typical limestone were used for the
 278 voussoirs. In addition, well-compacted sandy gravel were applied as backfill material. The material
 279 parameters were summarized in Table 2. Although geotechnical materials show significant variability,
 280 there was no intention to incorporate this effect in the present paper. Mortar joints between voussoirs
 281 were represented as zero thickness interfaces. In this study, considering that we are dealing with ageing
 282 low bond strength masonry, the tensile and cohesive resistance of the mortar was neglected and assumed
 283 equal to zero. Only frictional sliding between the voussoirs was allowed to occur. Similarly, only
 284 frictional resistance was allowed at the interface between the voussoirs and the backfill material. Table
 285 3 shows the material properties used for the development of the contact model. Contact normal stiffness
 286 was chosen sufficiently high value to avoid significant interpenetration between the elements. Friction
 287 angles between voussoirs and for the voussoir-soil interface were chosen according to guidelines [3].

288

289 Table 2 – Material parameters used in the numerical model.

Material	Density	Young modulus	Poisson's ratio	Friction angle	Cohesion	Tensile strength
Voussoirs	2500 kg/m ³	20 GPa	0.20	-	-	-
Foundation	2500 kg/m ³	20 GPa	0.20	-	-	-
Backfill	2000 kg/m ³	0.20 GPa	0.25	37°	5 kPa	5 kPa
Subsoil	2000 kg/m ³	5 GPa	0.25	50°	500 kPa	500 kPa

290

291

Table 3 – Contact parameters at the interfaces

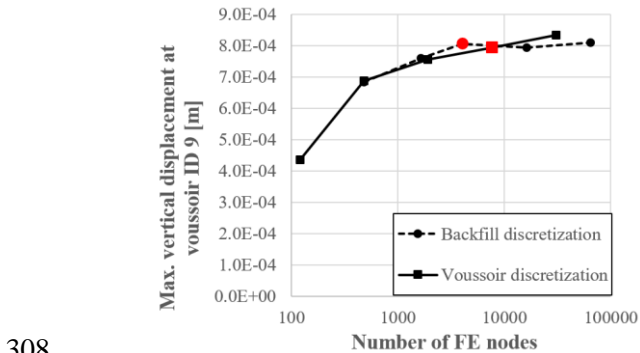
Contact location	Contact stiffness	Friction angle
Voussoir to voussoir	100 GPa/m	40°
Backfill to arch barrel	100 GPa/m	20°
Backfill to subsoil	100 GPa/m	20°

292

293 4.2. Finite Element discretization and boundary conditions

294 UDEC is using a constant-strain triangular finite elements by default. These elements can behave
 295 excessively stiff in plane-strain problems where plastic failure occurs. Plane-strain geometries can
 296 introduce a kinematic restraint in the out of plane direction, often giving rise to overprediction of the
 297 collapse load. To eliminate the non-physical hourglass modes of deformation, a discretization scheme
 298 proposed by Marti and Cundall [43] was used. In the applied discretization scheme, the discretization
 299 for the isotropic part of the strain and stress tensors differs from the discretization for the deviatoric part.

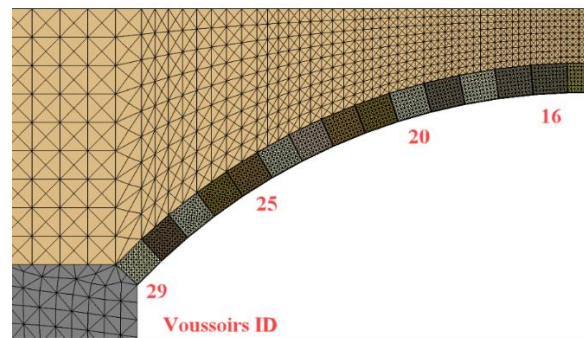
300 Moreover, to obtain accurate stress distribution in the voussoirs, a detailed discretization of the voussoirs
 301 implemented. In particular, the number of point contacts between the voussoirs was set high to ensure
 302 the accurate calculation of contact stresses. Convergence tests were carried out on the model to
 303 determine the appropriate number of finite elements for the voussoirs and for the backfill (Figure 5a).
 304 As a result, every voussoir was divided into 8×8×4 finite elements (Figure 5b), while the density of the
 305 FE mesh for backfill was assigned to be more dense above the crown (i.e. edge length ~5 cm) and coarser
 306 towards the sides of the model (i.e. edge length ~20 cm). The applied discretization is marked with red
 307 colour in Figure 5a.



308

309

(a)



(b)

310 Figure 5 – Finite element mesh for voussoirs and for backfill used for the development of the
 311 numerical model

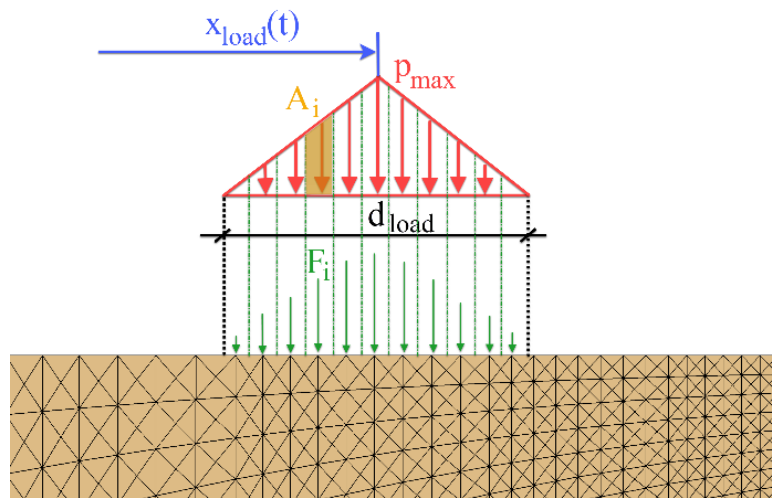
312 On the external boundaries, the velocity of the finite element nodes was set to zero. The boundaries of
 313 the model were defined sufficiently far from the structure to avoid the reflection of stresses from the
 314 boundaries during dynamic simulations. Moreover, non-reflecting viscous boundary was applied at the
 315 boundaries of the model.

316 The present paper neglects the presence of the track. In reality, it can be assumed that the train transmits
 317 its concentrated loads to the rail. These loads are dispersed by the sleepers and the ballast. It is assumed
 318 that the load is distributed on a $d_{load} = 1.0$ m loaded length. Triangular distribution was selected to ensure
 319 numerical stability (Figure 6).

320 The maximum intensity of distributed load was calculated using the equation below:

$$p_{max} = \frac{2R_y}{d_{load}}, \quad (13)$$

321 where R_y is the resultant of the external load, d_{load} is the length where the resultant force was
 322 distributed.



323

324

Figure 6 – Distribution of the external load

325 4.3. Types of analysis performed

326 Both static and dynamic analysis were carried out. The aim of dynamic analysis was to determine the
 327 dynamic response of the bridge. Moreover, investigations on the effect of magnitude of the external load
 328 on the dynamic amplification were made. In every simulation, as an initial step, the self-weight of the
 329 structure was assigned and equilibrated. Criterion for equilibrium was defined as the ratio of the average
 330 unbalanced mechanical force magnitude divided by the average applied mechanical force magnitude for
 331 all grid-points in the model. When this ratio was lower than $1.0e-6$, the structure was considered to be
 332 in equilibrium. At this stage, nodal velocities typically lower than $2.0e-6$ m/s. Near to the state of failure,
 333 convergence of the numerical model decreases significantly. Therefore, another limit was introduced as:
 334 *if the state of equilibrium cannot be reached within 300,000 calculation cycles in a single loading step,*
 335 *then the simulation was stopped and the corresponding load was considered as the failure load.*

336 4.3.1. Incrementally increased load at fixed positions along the span of the bridge (Type 1)

337 Experimental and field tests carried out on full-scale masonry arch bridges are typically using vertical
 338 loads at quarter span to gain information about the structural stiffness and load bearing capacity. The
 339 advantage of using numerical simulations is that models can be developed in which parametric studies
 340 can be carried out e.g. load can be applied in several loading positions in the bridge. In this study,
 341 numerical models have been carried out in which the load position has been varied along the span of the
 342 bridge. The procedure was as follows (Figure 7b): After a fixed x/s load position was selected (in which
 343 x is the distance from the edge of the arch ring of the bridge and s is the span of the bridge); the
 344 distribution of the load was defined according to Figure 6, while the magnitude of the vertical load was
 345 incrementally increased (i.e. load increment: 1.0 kN/m) until the structure failed. The simulation was
 346 repeated in nine different loading positions, i.e. from $x/s = 0.0$ until $x/s = 8/16$. In this way, load

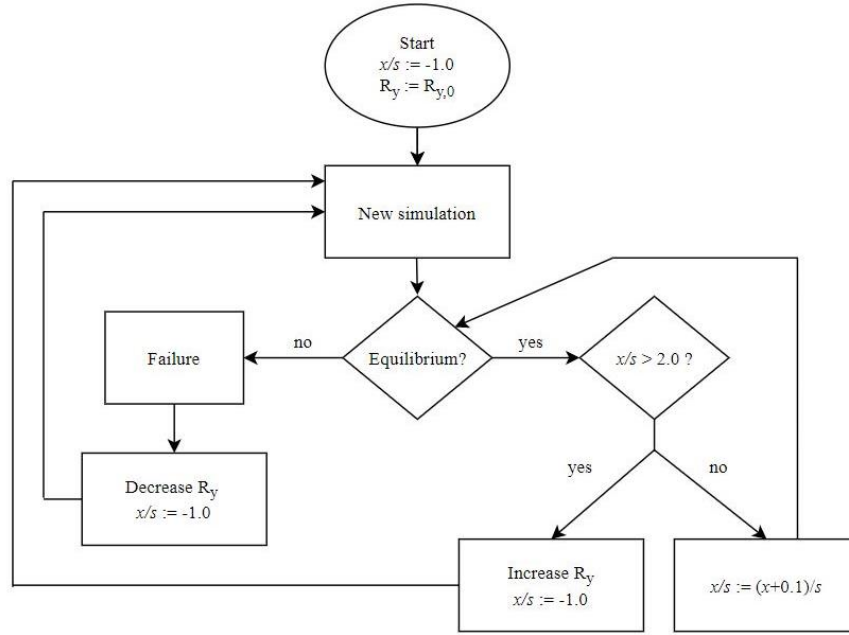


Figure 8 – Flowchart for quasi-static moving load analysis (Type 2)

4.3.3. Dynamic analysis (Type 3)

During the dynamic analysis the artificial damping and mass scaling were not applied during simulations. Energy dissipation can develop within the model via frictional sliding (e.g. at the extrados of the arch barrel where backfill can slide upon the voussoirs) or via the plastic deformations of the backfill material. As a conservative assumption, Rayleigh damping was not applied during the analysis. The external load was dragged through on the bridge with constant horizontal velocity (investigated range was between 10 to 120 m/s). Simulations were ended when: (i) the external load could cross the bridge and reached $x/s = 1.60$ without causing failure; or (ii) during the simulation the bridge failed. These simulations were repeated with different magnitude of external load.

During the analysis, radial displacements of each voussoir, maximal contact stresses at the inner and the outer side of the bed joints were recorded and plotted against the position of the external load. Dynamic response of the structure was compared to the static response and dynamic amplification factors obtained. Two types of dynamic amplification factor was evaluated. These are: (a) global dynamic amplification factor (DAF_{global}), where the highest dynamic response of the structure was selected and compared with the highest static response; and (b) local dynamic amplification ($DAF_{local,i}$) was defined for every voussoir as the highest dynamic response of the selected element compared to the static response of the same element:

$$DAF_{global} = \frac{\max_i |y_{dyn,i,max}|}{\max_j |y_{stat,j,max}|} \quad i, j = \{1 \dots \text{number of voussoirs}\}, \quad (14)$$

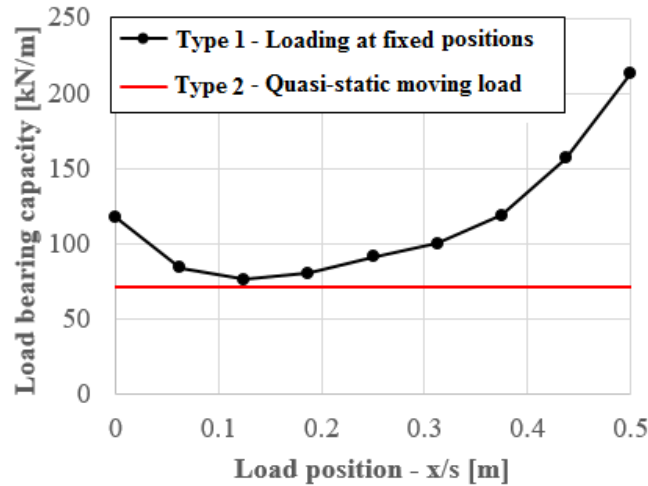
$$DAF_{local,i} = \frac{|y_{dyn,i,max}|}{|y_{stat,i,max}|} \quad i = \{1 \dots \text{number of voussoirs}\}, \quad (15)$$

where $y_{dyn,i,max}$ is the maximal dynamic and $y_{stat,i,max}$ is the maximal static response of the i^{th} element in a single simulation, respectively.

385 **5. Results**

386 **5.1. Results of the static analysis (Type 1 and 2)**

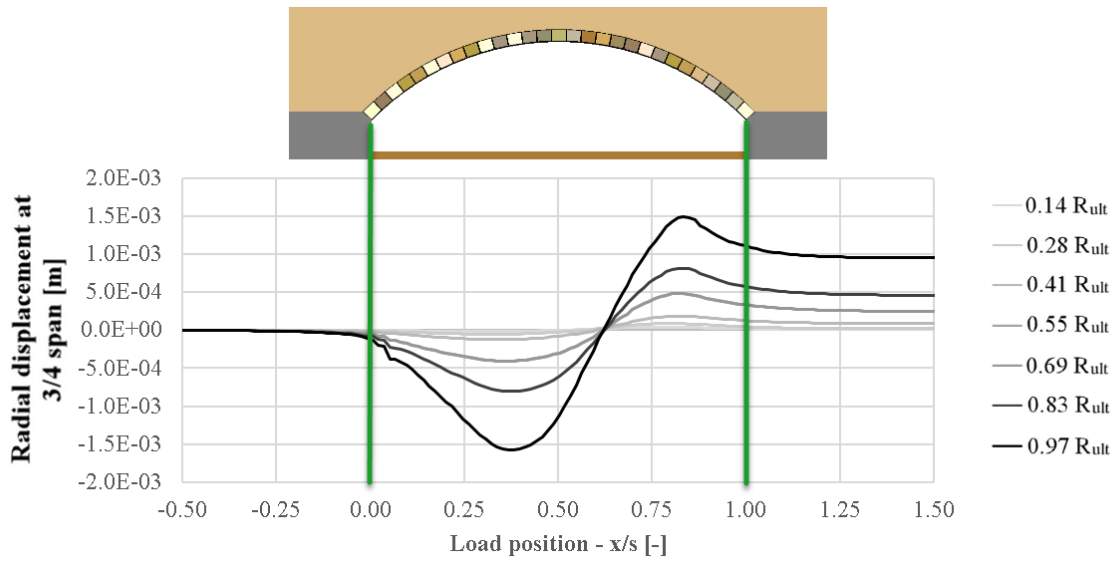
387 To get a first impression of the structural behaviour of the masonry arch bridge under investigation, the
388 failure load under static conditions was determined. With respect to the load bearing capacity, Type 2
389 analysis of moving load showed lower ultimate load by 7% (~71 kN/m) compared to Type 1 analysis
390 (~76 kN/m). The difference might be attributed partly due to the precision of the loading procedure, i.e.
391 the load increment was 1.0 kN/m; which can cause +/-1.5% error difference. Moreover, in the case of
392 quasi-static moving load, the load path/load history could cause weaker behaviour by non-elastic
393 deformation of the system. Type 2 simulation at ultimate load stopped at $x/s = 0.14$, which is close to
394 the critical position obtained from Type 1 simulation ($x/s = 0.125$).



395
396 Figure 9 – Ultimate load bearing capacity of the bridge

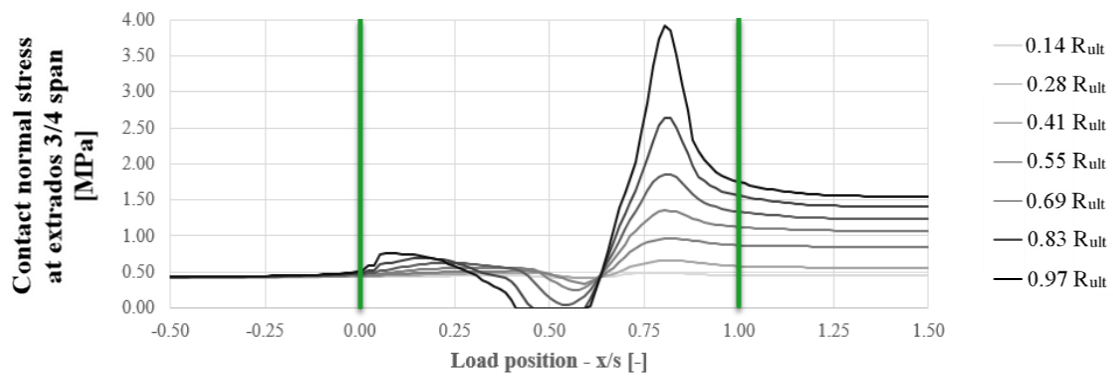
397 With respect to Type 1 analysis, load-deflection curves were obtained. Such analyses can be used to
398 determine the stiffness of the bridge. On the other hand, Type 2 analysis can provide valuable
399 information about the response (e.g. stresses, displacements) of the structure when the load of the vehicle
400 is passing from the bridge. Figure 10a-c shows the influence lines for radial displacements and contact
401 normal stresses at $\frac{3}{4}$ span of the bridge. With the increasing magnitude of external loads, contacts can
402 open (the normal stress decreases to 0 MPa) and close. Maximum contact stresses from influence lines
403 in Figure 10b-c were plotted against the ratio of external load magnitude divided by the ultimate load
404 (Figure 11). It was found that the maximum of the contact stress increases exponentially as the load
405 increases.

406



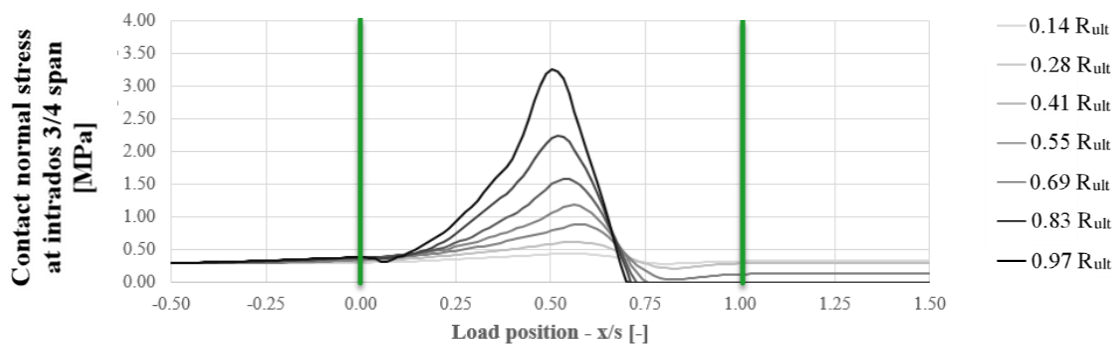
407
408

(a)



409
410

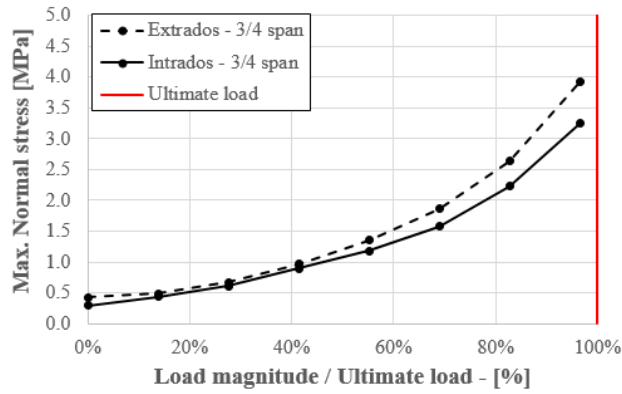
(b)



411
412

(c)

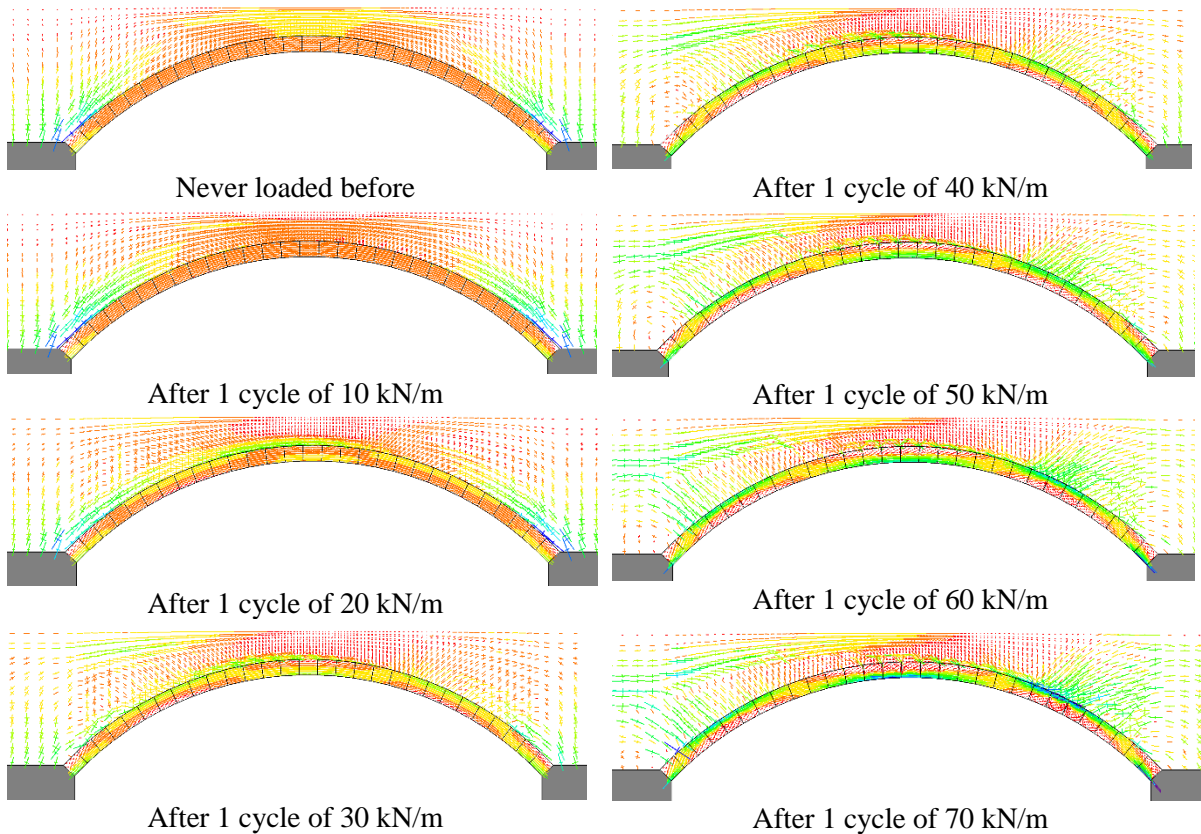
413 Figure 10 - Influence lines for voussoir at $\frac{3}{4}$ span: (a) radial displacements; (b) contact stresses
414 extrados side and (c) contact stresses at intrados side (Type 2 analysis)



415
416

Figure 11 – Maximum contact normal stress at $\frac{3}{4}$ span.

417 After the axle load passed through the bridge, the stresses within the structure went through
 418 redistribution: e.g. at $0.55R_{ult}$ (40 kN/m) and above a crack appeared (normal stress decreased to 0 Pa)
 419 and remained open at $\frac{3}{4}$ span intrados after the load left the bridge. Figure 12 represents the residual
 420 stress state of the arch barrel and the backfill after one cycle of external load passed through the structure
 421 when loaded under a quasi-static manner. The residual stress state depends on the magnitude of the
 422 external load. The arch barrel of the “never loaded” structure shows uniform normal stress distribution
 423 and the stresses between the voussoirs of the arch are in compression. As the magnitude of the external
 424 load increases, the residual stress state of arch barrel contains significant bending as well.



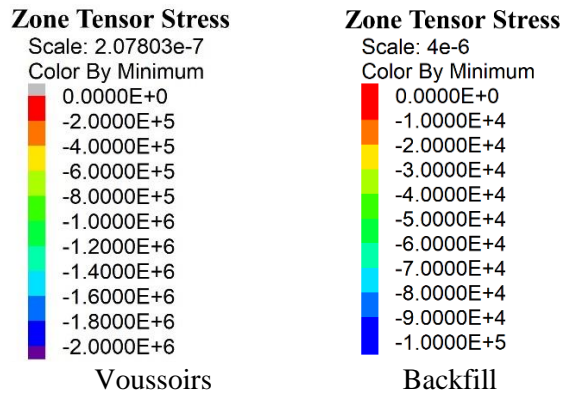
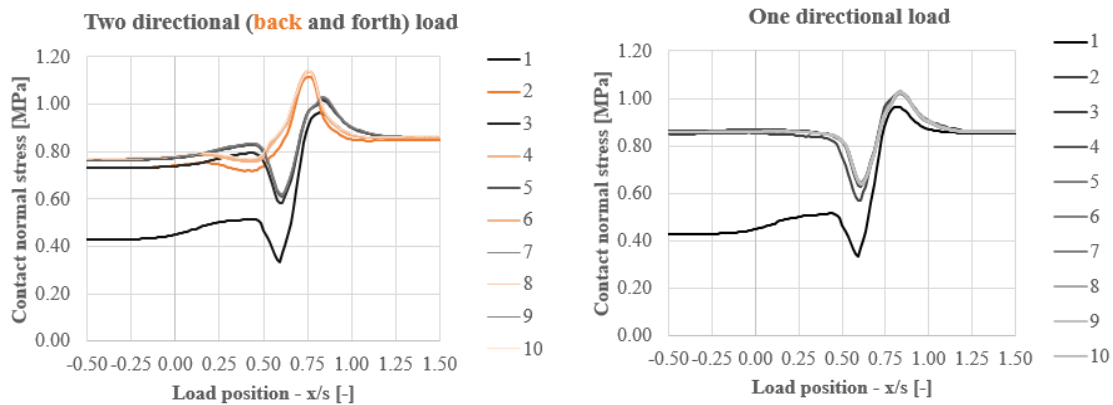
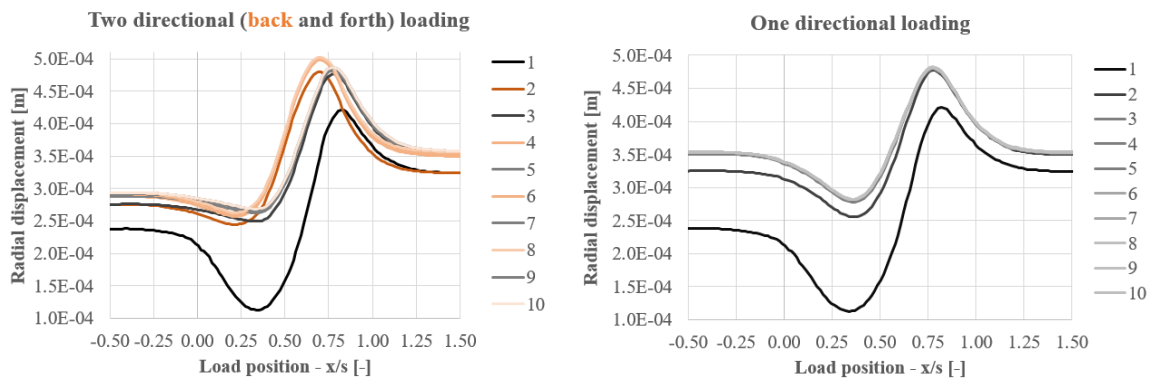


Figure 12 – Residual stress state after one cycle of external load crossed the structure (negative values mean compression – Type 2 analysis)

425 Axle loads follow each other simultaneously and trains would cross the bridge typically in both
 426 directions (i.e. left to right and right to left). Figure 13 shows the normal stresses at $\frac{3}{4}$ span (extrados
 427 side), while the axle load ($R_y = 30 \text{ kN/m} = 0.42R_{ult}$) crossed the bridge 10 times. The distance between
 428 the loads was chosen sufficiently large to avoid interaction between the loads). According to Figure 13,
 429 after the third cycle, additional redistribution of the stresses cannot be observed. Also, when the moving
 430 load is in backward direction, we have redistribution of stresses and maximum displacement occurs at
 431 different load position, see Figure 14a. Convergence to the shakedown state was slower in case of two
 432 directional and faster in case of one directional loading.

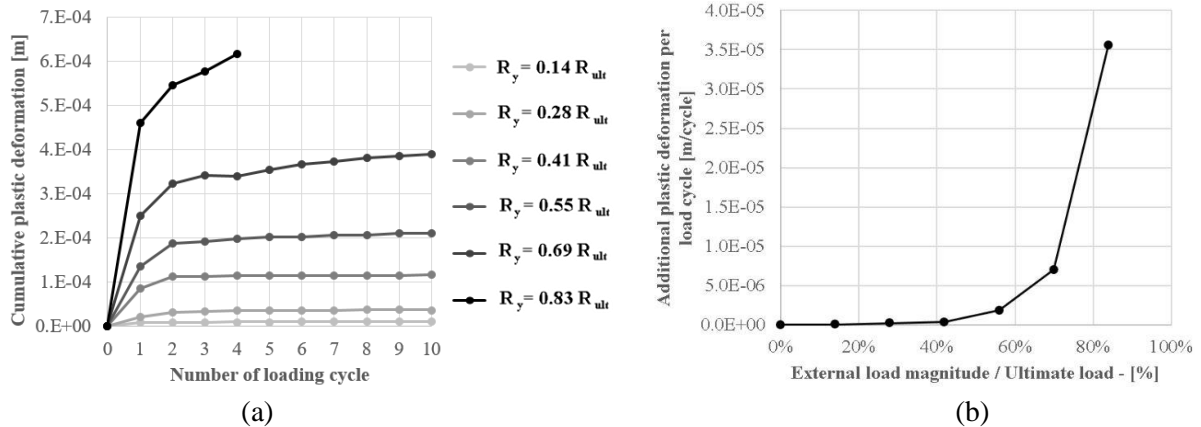


433
 434 Figure 13 – Repeated loading ($R_y=30 \text{ kN/m} = 0.42 R_{ult}$): influence lines for contact normal stress at $\frac{3}{4}$
 435 span extrados: (a) two-directional; (b) one directional load path



436
 437 Figure 14 – Repeated loading ($R_y = 30 \text{ kN/m} = 0.42 R_{ult}$): influence lines for radial displacements at $\frac{3}{4}$
 438 span: (a) two-directional; (b) one directional load path

439 Simulations with repeated, one directional quasi-static loading were done with several external load
 440 magnitudes. If the magnitude of the external load does not exceed the ~50% of the ultimate load, then
 441 plastic deformations cease after 2-3 initial cycles and the response of the structure goes back to pure
 442 elastic with some state of residual stresses (Figure 15a-b). Similar shakedown phenomena was observed
 443 previously during the experimental test of masonry arches [44, 45]. Above ~50% of R_{ult} , additional
 444 plastic deformations were observed in every cycle of repeated loading. Also, at 85% of R_{ult} , equilibrium
 445 was not reached after the fourth cycle which means that the structure has failed. It is worth to mention,
 446 that according to Figure 15a, the bridge which seemed to have sufficient resistance for $0.83R_{ult}$,
 447 collapsed after the fourth cycle of loading with the same loading magnitude.

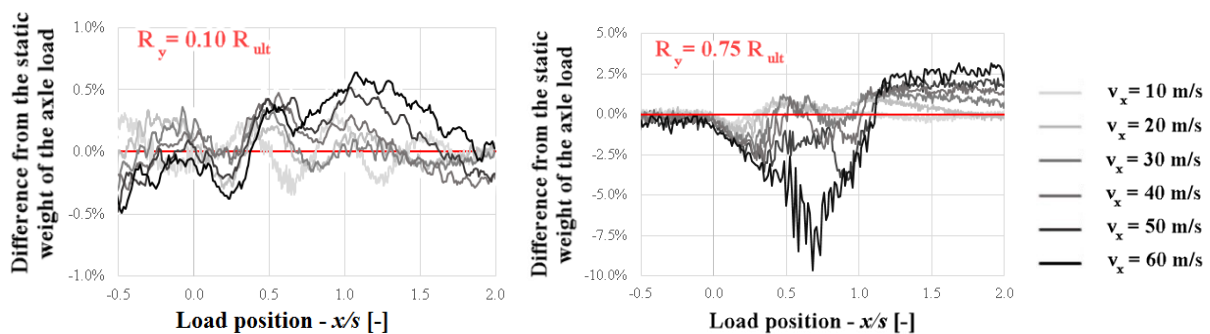


448
 449
 450 Figure 15 – Plastic shakedown of masonry arch bridge: (a) cumulative plastic deformation at $\frac{3}{4}$ span,
 451 (b) additional plastic deformations in a single load cycle

452

453 5.2. Results of dynamic analysis (Type 3)

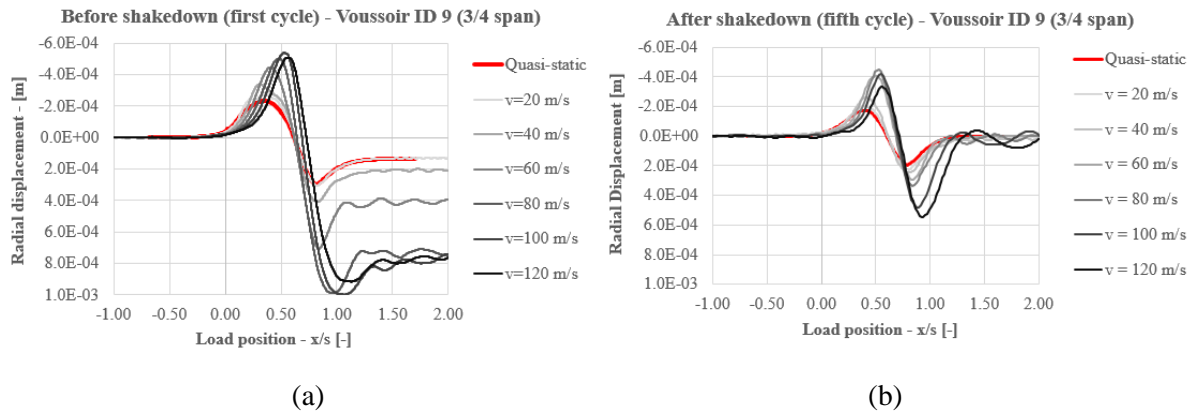
454 In the dynamic analysis, the effect of vehicle-structure interaction was investigated. From the results
 455 analysis it was found that the vehicle-structure interaction is not significant i.e. the contact force between
 456 the track and the vehicle does not change significantly as the load passing through (Figure 16). This
 457 finding is in accordance with the EN 1991-2 and can be explained with significantly higher mass of the
 458 structure compared to the mass of the vehicle. As the magnitude of the external load gets closer to the
 459 ultimate load bearing capacity, the difference between the static and the dynamic contact force is
 460 increasing.



461
 462 Figure 16 – Dynamic contact forces between the track and the vehicle

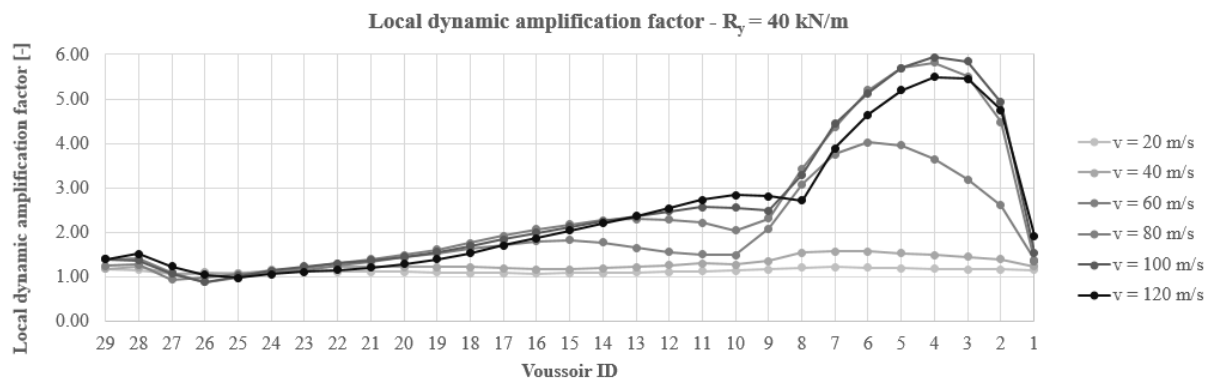
463 Also, as described in Section 4.3.3, dynamic analysis was carried out to obtain dynamic amplification
 464 factors and compared them with the multiplication factors calculated according to Network Rail
 465 standards. The investigated range of horizontal velocities was 10 m/s to 120 m/s. To decouple the
 466 phenomena of the plastic shakedown and the dynamic enhancement and exclude plastic deformations
 467 in the structure, all of the dynamic simulation was repeated 5 times, see Figure 17a-b. Moreover,

468 influence lines for radial displacements at $\frac{3}{4}$ span ($R_y=40 \text{ kN/m}=0.55R_{ult}$) were plotted and are shown
 469 in Figure 17b. As the velocity of the load increased and reached 100 m/s, radial displacements increased
 470 as well. On the other hand, for train speeds greater than 100 m/s, displacements in the structure
 471 decreased. The maximum response of the structure has a “delay” as the velocity increases compared to
 472 quasi-static analysis. The maximum value of outward (negative) radial displacement occurs when the
 473 load is at $x/s = 0.33$ in case of quasi-static analysis, while it is around $x/s = 0.55$ when the velocity
 474 is 120 m/s.



475
 476 (a) (b)
 477 Figure 17 – Influence lines for radial displacements at $\frac{3}{4}$ span ($R_y=40 \text{ kN/m}$): (a) dynamic behaviour
 478 in the first loading cycle - before shakedown; (b) dynamic behaviour after shakedown

479 Radial displacement of every voussoir in the arch barrel was recorded and local dynamic amplification
 480 factors according to Eq (15) were calculated. From Figure 18 the DAF values are different at different
 481 parts of the arch barrel. The difference is increasing as the velocity of the external load is increasing. At
 482 Voussoir ID 1-8, significantly higher local DAFs were calculated. It should be noted, that the static
 483 response of the structure was very low at this part of the bridge.

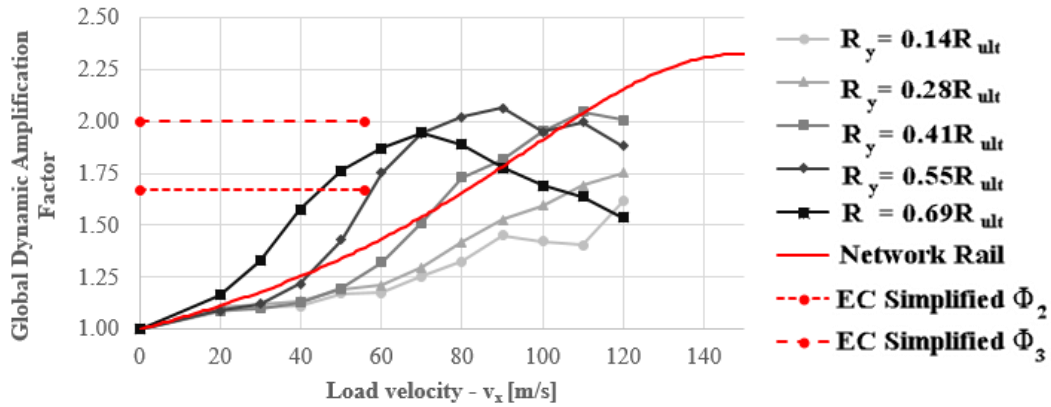


484
 485 Figure 18- Local dynamic amplification factors for displacements at $R_y=40 \text{ kN/m}$

486 Dynamic amplification factors for displacements were calculated from Figure 17b and plotted in Figure
 487 19. Moreover, simulations were repeated with different magnitude of external loads. The highest value
 488 of global DAF was around 210%. Critical speed – where the DAF has the highest value at a given
 489 magnitude of external load – is decreasing as the magnitude of the external load gets close to the ultimate
 490 load. Similarly, the highest value of DAF is slightly decreasing at higher level of external loads.

491 To compare the numerically obtained DAF with the ones given in guidelines, the natural frequency of
 492 the structure investigated in this work was determined with modal analysis. From the investigations, it
 493 was shown that the first natural frequency was $\sim 30,5 \text{ Hz}$, which is between the limits of EN 1991-2
 494 simplified method, hence the code is applicable $\Phi_2 = 1.67$ and $\Phi_3 = 2.00$. The dynamic enhancement

495 according to the Network Rail standard (Eqs. 3 and 4) was calculated and shown in Figure 19. In the
 496 case of lower load levels ($<40\% R_{ult}$), the formulas of the Network Rail provides a reasonably precise
 497 and safe estimate for DAFs. It should be noted, that if the external load is closer to the ultimate load
 498 bearing capacity, then the standard can underestimate the dynamic enhancement. From Figure 19 and
 499 Table 4, it is evident, that the critical speed (where the DAF value is the highest) is decreasing as the
 500 magnitude of the external load is increasing. This phenomena can be explained by the nonlinear
 501 behaviour of the structure: at higher load levels, the bridge starts to behave softer, hence the natural
 502 frequency of it is decreasing which is resulted in lower critical speeds.



503
 504 Figure 19 – Global Dynamic Amplification Factors for displacements at different level of external
 505 load

506

507 Table 4 – Critical speed at various load levels

External load level	Critical speed [m/s]
$0.14R_{ult}$	>120 m/s
$0.28R_{ult}$	>120 m/s
$0.41R_{ult}$	110 m/s
$0.55R_{ult}$	90 m/s
$0.69R_{ult}$	70 m/s

508

509

510 6. Conclusions

511 The structural assessment of masonry arch bridges is of great importance due to their long service life
512 and deterioration condition over time. Dynamic amplification factor (DAF) is a parameter which
513 accounts for the dynamic impact of moving trains on structures by relating the static to the dynamic
514 characteristics of a bridge. Although, accurate prediction of the DAF can provide valuable information
515 related to sustainable management of bridges, the structural assessment of the dynamic characteristics
516 of masonry arch bridges and predictions of DAFs are rather difficult to be obtained. This is mainly due
517 to the complexity of the problem and that recent studies have reported contradictory results. This paper
518 focuses on the shakedown and dynamic behaviour of railway masonry arch bridges under traffic load
519 conditions. A nonlinear, mixed discrete-finite element was developed to investigate the static and
520 dynamic response of the Prestwood masonry arch bridge. Each voussoir of the masonry arch was
521 represented by a distinct block. Mortar joints were modelled as zero thickness interfaces which can open
522 and close depending on the magnitude and direction of the stresses applied to them. The numerical
523 model was calibrated based on field full-scale experimental test results. The bridge was subjected to two
524 different types of static analysis and a real dynamic analysis to simulate the effects of moving load.
525 Investigations into the train to bridge interaction was also undertaken. Finally, the local and global
526 Dynamic Amplification Factors were studied. The major findings of the work can be summarized as
527 follows:

- 528 - Failure load of the investigated structure was determined in two different ways i.e. with
529 monotonically increased loads at fixed positions and with quasi-static moving loads. From the
530 results analysis it was shown that the latter reflects better the characteristic of real traffic since
531 can take into account the interaction between the adjacent load positions. The load bearing
532 capacity was 7% lower (71 kN/m) in case of “quasi-static moving load” type loading.
- 533 - As the external load passes through the bridge, plastic deformations and residual stresses exist
534 in the arch barrel. If the magnitude of the external load does not exceed the 50% of the ultimate
535 load bearing capacity, the plastic deformations cease after 2-3 cycles of external load and the
536 structure is in a shakedown state. If the magnitude of the external load exceeds the 50% of the
537 ultimate load, continuous plastic deformations were experienced in the loading cycles.
- 538 - With increasing load magnitude, the maximum contact normal stresses between the voussoirs
539 are increasing exponentially.
- 540 - A single degree of freedom vehicle-structure interaction was developed and integrated within
541 the developed code. Numerical experiences suggested, that vehicle-structure interaction has a
542 negligible effect on the global behaviour of the bridge.
- 543 - Local and Global Dynamic Amplification Factors were introduced to have deeper insight into
544 the dynamic enhancement. At different parts of the arch barrel, different magnitude of DAF was
545 measured. It was shown that the dynamic amplification depends on the magnitude of the
546 external load. As the load increases, non-linearity in the structural behaviour is evident, which
547 decreases the natural frequency of the bridge. Hence the critical speed (i.e. where the highest
548 DAF value can be measured) is decreasing.
- 549 - In the case of typical service load levels ($<40\% R_{ult}$), the formulas of the Network Rail provides
550 a reasonably precise and safe estimate for DAFs. For this particular type of structure, for a
551 service load greater than $40\% R_{ult}$ the Network Rail formulas underestimate DAFs.

552 Limitation of the current work is that it neglects those structural element of a masonry bridge (e.g
553 spandrel walls) which makes the structural behaviour three-dimensional. Moreover, further
554 experimental studies will be needed to investigate the effect of geometry on the dynamic behaviour of
555 masonry arch bridges to obtain more general results. Results presented from this study can improve
556 understanding of the dynamic behaviour of masonry arch bridge and inform repair and maintenance
557 schemes.

558 **Acknowledgements**

559 The authors express their gratitude to the ITASCA Education Partnership Program for providing a copy
560 of UDEC software to assist the above research. The work presented in this paper was partially financially
561 supported by an EPSRC doctoral training award (CASE/179/65/82).

562 **References**

- 563 [1] UIC. Code UIC 776-1R - Charges à Prendre en Considération Dans le Calcul des Ponts-Rails, 4e
564 edition. 1994.
- 565 [2] Page JJ, Britain) TRLG. Masonry arch bridges: HMSO; 1993.
- 566 [3] Jensen JS, Casas JR, Karoumi R, Plos M, Cremona C, Melbourne C. Guideline for load and
567 resistance assessment of existing european railway bridges. Fourth International Conference on Bridge
568 Maintenance, Safety and Management (IABMAS 08). France2008. p. pp 3658-65.
- 569 [4] State of the Nation 2018: Infrastructure Investment. In: (ICE) IoCE, editor. UK: Institution of Civil
570 Engineers (ICE); 2018. p. 31.
- 571 [5] Pippard AJS, Tranter E, Chitty L. The Mechanics of the Voussoir Arch. Journal of the Institution of
572 Civil Engineers. 1936;4:281-306.
- 573 [6] Wang J, Haynes B, Melbourne C. A comparison between the MEXE and Pippard's methods of
574 assessing the load carrying capacity of masonry arch bridges. ARCH'13 Proceedings of the 7th
575 International Conference on Arch Bridges Trogir-Split, Croatia October 4-6, 2013: SECON-CSSE,
576 Zagred, Croatia.; 2013. p. 589-96.
- 577 [7] Audenaert A, Beke J. Applicability analysis of 2D-models for masonry arch bridge assessment: Ring,
578 Archie-M and the elasto-plastic model. WSEAS Transactions on applied and theoretical mechanics.
579 2010;5:221-30.
- 580 [8] Melbourne C, McKibbins L, Sawar N, Sicilia Gaillard C. Masonry arch bridges: condition appraisal
581 and remedial treatment. London: University of Salford, UK; 2006.
- 582 [9] Fanning PJ, Boothby TE. Three-dimensional modelling and full-scale testing of stone arch bridges.
583 Comput Struct. 2001;79:2645-62.
- 584 [10] Sarhosis V, De Santis S, de Felice G. A review of experimental investigations and assessment
585 methods for masonry arch bridges. Structure and Infrastructure Engineering. 2016;12:1439-64.
- 586 [11] Choo BS, Gong NG. Effect of skew on the strength of masonry arch bridges. Arch Bridges.
587 1995:205-14.
- 588 [12] Giamundo V, Sarhosis V, Lignola GP, Sheng Y, Manfredi G. Evaluation of different computational
589 modelling strategies for the analysis of low strength masonry structures. Engineering Structures.
590 2014;73:160-9.
- 591 [13] Boothby TE. Analysis of masonry arches and vaults. Progress in Structural Engineering and
592 materials. 2001;3:246-56.
- 593 [14] Sarhosis V, Garrity SW, Sheng Y. Influence of brick-mortar interface on the mechanical behaviour
594 of low bond strength masonry brickwork lintels. Engineering Structures. 2015;88:1-11.
- 595 [15] Moradabadi E, Laefer DF, Clarke JA, Lourenço PB. A semi-random field finite element method to
596 predict the maximum eccentric compressive load for masonry prisms. Constr Build Mater. 2015;77:489-
597 500.
- 598 [16] Lemos JV. Discrete Element Modeling of Masonry Structures. International Journal of
599 Architectural Heritage. 2007;1:190-213.
- 600 [17] Zhang YY, Macorini L, Izzuddin BA. Numerical investigation of arches in brick-masonry bridges.
601 Structure and Infrastructure Engineering. 2018;14:14-32.
- 602 [18] Forgács T, Sarhosis V, Bagi K. Influence of construction method on the load bearing capacity of
603 skew masonry arches. Engineering Structures. 2018;168:612-27.
- 604 [19] Gago A, Alfaiate J, Gallardo A. Numerical analyses of the Bargower arch bridge. Finite elements
605 in civil engineering applications Lisse (Tokyo): Swets & Zeitlinger. 2002.
- 606 [20] Ford T, Augarde C, Tuxford S. Modelling masonry arch bridges using commercial finite element
607 software. 9th International Conference on Civil and Structural Engineering Computing, Egmond aan
608 Zee, The Netherlands2003. p. 2-4.
- 609 [21] Drosopoulos G, Stavroulakis G, Massalas C. Limit analysis of a single span masonry bridge with
610 unilateral frictional contact interfaces. Engineering Structures. 2006;28:1864-73.

- 611 [22] de Felice G. Assessment of the load-carrying capacity of multi-span masonry arch bridges using
612 fibre beam elements. *Engineering Structures*. 2009;31:1634-47.
- 613 [23] De Santis S, de Felice G. A fibre beam-based approach for the evaluation of the seismic capacity
614 of masonry arches. *Earthq Eng Struct D*. 2014;43:1661-81.
- 615 [24] Cundall PA. A computer model for simulating progressive, large-scale movements in blocky rock
616 systems. *Proc Int Symp on Rock Fracture*. 1971:11-8.
- 617 [25] Mirabella R, Calvetti E. Distinct element analysis of stone arches. Sinopoli (ed), *Arch Bridges;*
618 *Proc Intern Symp, Paris1998*. p. 6-9.
- 619 [26] Toth AR, Orban Z, Bagi K. Discrete element analysis of a stone masonry arch. *Mech Res Commun*.
620 2009;36:469-80.
- 621 [27] Sarhosis V, Sheng Y. Identification of material parameters for low bond strength masonry.
622 *Engineering Structures*. 2014;60:100-10.
- 623 [28] Eurocode 1: Actions on structures–Part 2: Traffic loads on bridges. 2003.
- 624 [29] Rail N. The structural assessment of underbridges. Network Rail, London, UK, Guidance Note
625 NR/GN/CIV/025. 2006.
- 626 [30] Smith J, Acikgoz S. Dynamic Amplification of Curved Beams Subjected to a Moving Point Load.
627 2020. p. 212-20.
- 628 [31] Costa C, Arêde A, Costa A. Numerical simulation of stone masonry arch bridges behaviour under
629 road traffic moving loads. *Proceedings of ARCH'10-the 6~(th) International Conference on Arch*
630 *Bridges2010*.
- 631 [32] Jorge P, Ribeiro D, Costa C, Arêde A, Calçada R. Train-bridge dynamic interaction on a stone
632 masonry railway bridge2016.
- 633 [33] Silva R, Costa C, Arêde A. Nonlinear Analysis of a Multispan Stone Masonry Bridge Under
634 Railway Traffic Loading. *International Conference on Arch Bridges: Springer; 2019*. p. 119-27.
- 635 [34] Rafiee-Dehkharghani R, Ghyasvand S, Sahebalzamani P. Dynamic Behavior of Masonry Arch
636 Bridge under High-Speed Train Loading: Veresk Bridge Case Study. *J Perform Constr Fac*.
637 2018;32:04018016.
- 638 [35] Ataei S, Miri A. Investigating dynamic amplification factor of railway masonry arch bridges
639 through dynamic load tests. *Constr Build Mater*. 2018;183:693-705.
- 640 [36] D214/RP9 E. Railway bridges for speeds > 200 km/h. European Rail Research Institute (ERRI)
641 Utrecht; 2001.
- 642 [37] Ladislav F. *Dynamics of Railway Bridges*. 1996.
- 643 [38] ITASCA. UDEC - Universal Distinct Element Code Manual. Theory and Background. Mineapolis,
644 USA: Itasca Consulting Group; 2004.
- 645 [39] Sarhosis V, Forgács T, Lemos JV. A discrete approach for modelling backfill material in masonry
646 arch bridges. *Comput Struct*. 2019;224:106108.
- 647 [40] Forgacs T, Sarhosis V, Ádány S. Discrete Element Modeling of skew masonry arch bridges taking
648 into account arch ring-backfill interaction. In: Milani G, Taliercio A, Garrity S, editors. *10th*
649 *International Masonry Conference*. Milan, Italy2018.
- 650 [41] Forgács T, Rendes S, Ádány S, Sarhosis V. Mechanical Role of Spandrel Walls on the Capacity of
651 Masonry Arch Bridges. *International Conference on Arch Bridges: Springer; 2019*. p. 221-9.
- 652 [42] Page J. Load tests to collapse on two arch bridges at Preston, Shropshire and Prestwood,
653 Staffordshire. 1987.
- 654 [43] Marti J, Cundall P. Mixed discretization procedure for accurate modelling of plastic collapse. *Int J*
655 *Numer Anal Met*. 1982;6:129-39.
- 656 [44] Rosson BT, Søyland K, Boothby TE. Inelastic behavior of sand-lime mortar joint masonry arches.
657 *Engineering structures*. 1998;20:14-24.
- 658 [45] Boothby TE, Rosson BT. Elasto-plastic Hardening and Shakedown of Masonry Arch Joints.
659 *Meccanica*. 1999;34:71-84.